ELSEVIER

Ceramics International 29 (2003) 117–137

CERAMICS INTERNATIONAL

www.elsevier.com/locate/ceramint

Enhancement of the trapped-fields and mechanical properties of Nd–Ba–Cu–O bulk superconductors

M. Matsui[a,b,*], M. Murakami[a]

[a]*Superconductivity Research Laboratory, International Superconductivity Technology Center, 1-16-25 Shibaura, Minato-ku, Tokyo 105-0023, Japan*

[b]*Railway Technical Research Institute, 2-8-38, Hikari-cho, Kokubunji, Tokyo 185-8540, Japan*

Received 29 April 2002; received in revised form 5 May 2002; accepted 5 May 2002

Abstract

We have studied the effects of processing conditions and the initial compositions in Nd–Ba–Cu–O bulk superconductors on the field-trapping capability and the mechanical properties. Sintering the sample prior to the crystal growth was effective for the fabrication of a good quality sample with high trapped-fields. The optimization of Nd422 and Ag contents along with processing conditions led to an increase in both the field-trapping ability and mechanical properties. As a result, the trapped-field of Nd–Ba–Cu–O 30 mm in diameter reached 1.4 T at liquid nitrogen temperature. The average tensile strength and the Weibull coefficient exceeded 50 MPa and 13, respectively.

Keywords: B. Microstructure; C. Superconductivity; Trapped-field; Tensile strength; Bulk; Nd–Ba–Cu–O

1. Introduction

After the discovery of high temperature superconductors, intensive research has been carried out to seek for the melt-processing methods suitable for industrial applications. At an early stage of the research, bulk superconductors were fabricated with a sintering method, since the technique is commonly used for the synthesis of ceramic materials. However sintered oxide superconductors suffered from a weak-link problem at the grain boundaries. Melt-growth techniques [1,2] have solved such a weak-link problem through grain alignment. An addition of non-superconducting particles was also effective in increasing flux pinning. Later, the refinement of non-superconducting inclusions was achieved through the addition of Pt and CeO_2, which further increased the J_c values [3,4]. Recently, the J_c value in a self-field has reached the level of 10^5 A/cm^2 at 77 K [5,6]. In order to impart a high field-trapping ability, it is necessary to increase the size of a single domain besides high J_c. Hence, the crystal orientation was controlled by the top-seeded melt-growth (TSMG) technique using a *c*-axis aligned seed crystal with a higher decomposition temperature.

It is known that Y–Ba–Cu–O forms only a stoichiometric superconducting 123 phase [7,8]. Unlike Y123, RE123 (RE: Nd, Sm, Eu, Gd) is known to form a RE-Ba solid solution [8,9]. When RE123 compounds are synthesized in air, a large amount of RE elements substitute Ba site, leading to the degradation of superconducting properties [8,10]. Recent investigations revealed that superconducting properties were largely improved when the samples were synthesized under low oxygen partial pressure [11]. In particular, Nd–Ba–Cu–O (Nd123/Nd422) superconductors exhibited remarkable properties such as T_c of 95–96 K and high J_c accompanied by a large fishtail in a J_c–B curve [11], and hence they were considered to be promising materials to replace Y–Ba–Cu–O superconductors in various industrial applications.

In the Nd–Ba–Cu–O system, both $Nd_{1+x}Ba_{2-x}Cu_3O_{7-\delta}$ (Nd123ss) and $Nd_{4-x}Ba_{2+x}Cu_2O_{10}$ (Nd422ss) phases have a wide range of Nd–Ba solid solution [8–10,12]. Therefore, the superconducting properties of Nd–Ba–Cu–O superconductors are sensitive to the processing conditions such as the growth temperature [12]

* Corresponding author. Tel.: +81-3-3454-9284; fax: +81-3-3454-9287.

E-mail address: matsui@istec.or.jp (M. Matsui).

0272-8842/03/$22.00
PII: S0272-8842(02)00094-9

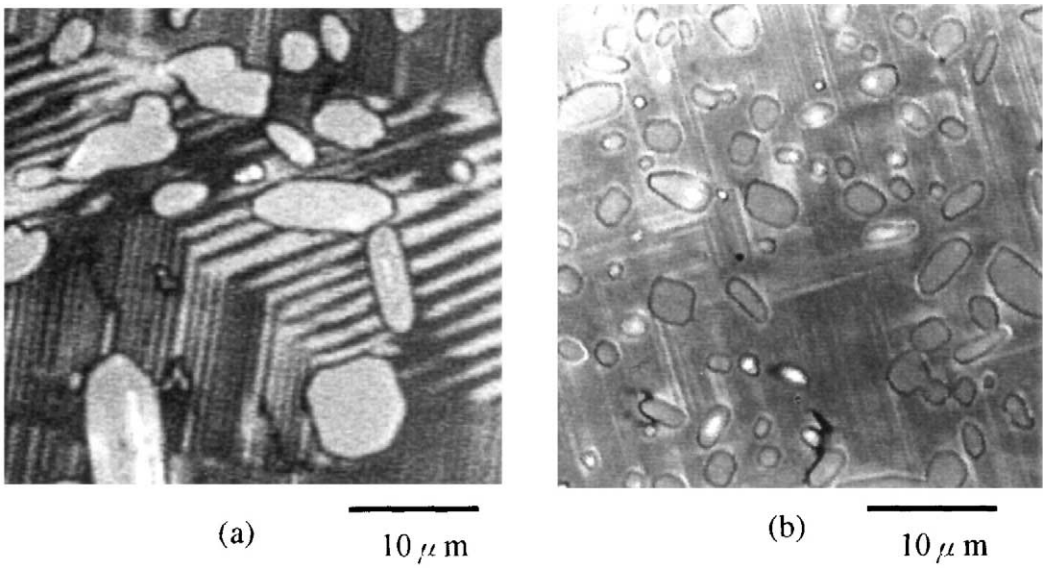

Fig. 1. Optical micrographs for the samples (a) without Ag addition and (b) with 10 wt.%Ag_2O addition. The initial molar ratio of Nd123:Nd422 is 10:2. The average sizes of Nd422 particles in the matrix were (a) 4.44 and (b) 2.33 μm.

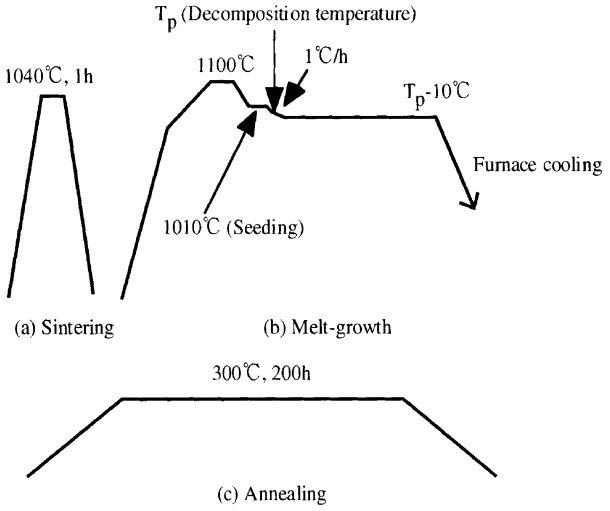

Fig. 2. Thermal schedules for the preparation of Nd–Ba–Cu–O bulk superconductors: (a) sintering, (b) melt-growth and (c) oxygenation. Sample A was not sintered while sample B was sintered before the melt-growth. Both samples were annealed in pure oxygen.

and the compositional fluctuation at the growth interfaces.

Furthermore, high T_c superconductors are brittle ceramic materials, and the field-trapping capability is often restricted by their poor mechanical properties [13,14]. The presence of normal conducting precipitates such as RE211, Nd422ss (Nd422 solid solution) and Ag particles affect the distribution of residual stress, and thereby mechanical performance of bulk superconductors. Although it was confirmed that Ag addition enhanced the mechanical strength of bulk superconductors [15–17], the effect of combined addition of 211(422) and Ag particles are still under discussion.

In this work, we fabricated Ag-doped large single-domain Nd–Ba–Cu–O superconductors with various initial compositions under different processing conditions with the aim of optimizing the processing conditions and the amount of Nd422 and Ag in regard to the field-trapping capability. We also studied the effect of Nd422 and Ag content on the mechanical properties.

2. Experimental

High-T_c single-domain bulk superconductors are usually synthesized by the TSMG technique. Nd bulks are also subjected to this method. However, the decomposition temperature of Nd system is highest among high-T_c 123 superconductors. Hence, there was not an appropriate candidate for a seed crystal with higher decomposition temperature. Although Lo et al. [18] attempted to fabricate Nd bulk with MgO seed crystal, it was difficult to control the crystal orientation due to the mismatch of the crystal lattice between MgO and Nd123. This was one of the factors that made it difficult to fabricate single-domain Nd bulks. Recently, several researchers reported one of Ag functions in a bulk sample was to decrease the decomposition temperature of Nd system [19], leading to the easier fabrication of Nd bulks. Furthermore, Fig. 1 shows the microstructures for the samples (a) without and (b) with Ag addition. In Nd system, Ag addition depressed the coarsening of Nd422 particles unlike other systems, suggesting that these particles play a better role in flux pinning. Accordingly, we fabricated Ag-doped Nd bulks 30 mm in diameter and 10 mm in thickness using Nd seed crystals

Fig. 3. Photo of sample A. Sample A was not sintered in pure oxygen before the crystal growth.

without Ag addition in flowing 1%O_2-Ar atmosphere. The detailed experimental procedures are as follows.

We prepared precursor Nd–Ba–Cu–O powders with various nominal compositions. After thorough mixing, the powders were pressed into pellets 40 mm in diameter and subjected to cold isostatic pressing. First, the pellets with the nominal composition of Nd123:Nd422 = 10:2 + 10 wt.%Ag_2O were employed to investigate the effect of sintering prior to melt-processing on the superconducting properties and the field-trapping capabilities.

Fig. 2 shows the thermal schedules for the preparation of Nd–Ba–Cu–O bulk superconductors. Sample A was grown using the TSMG technique with a Nd123 seed crystal in flowing 1%O_2-Ar atmosphere without sintering before melt-processing. Sample B was sintered at 1040 °C for 1 h in pure oxygen and then processed by

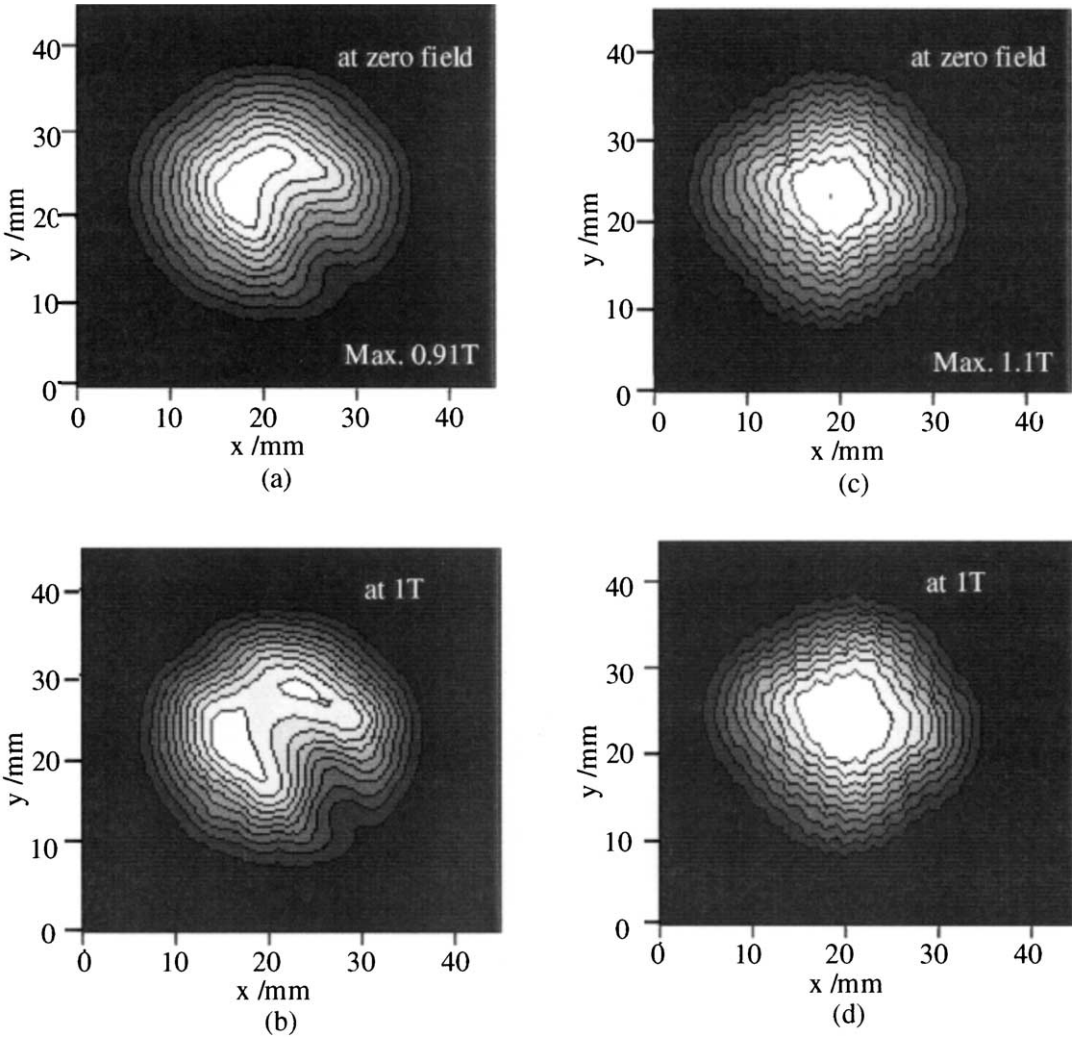

Fig. 4. Field distributions trapped by samples A and B at liquid nitrogen temperature: (a) A in the remnant state: (b) A in 1T; (c) B in the remnant state; (d) B in 1T.

the TSMG method. The grown crystals were oxygenated at 300° for 200 h. The densities of a precursor pellet, a sintered pellet and a grown crystal were measured to investigate the effect of sintering. The trapped magnetic fields were measured in liquid nitrogen using a Hall sensor, which was scanned 1 mm above the top surface. The maximum trapped-field values were measured by attaching a Hall sensor directly on the sample surfaces. The field dependencies of the maximum trapped-field values for the grown blocks were also measured. Small specimens cut from grown bulks were subjected to DC magnetization measurements using a

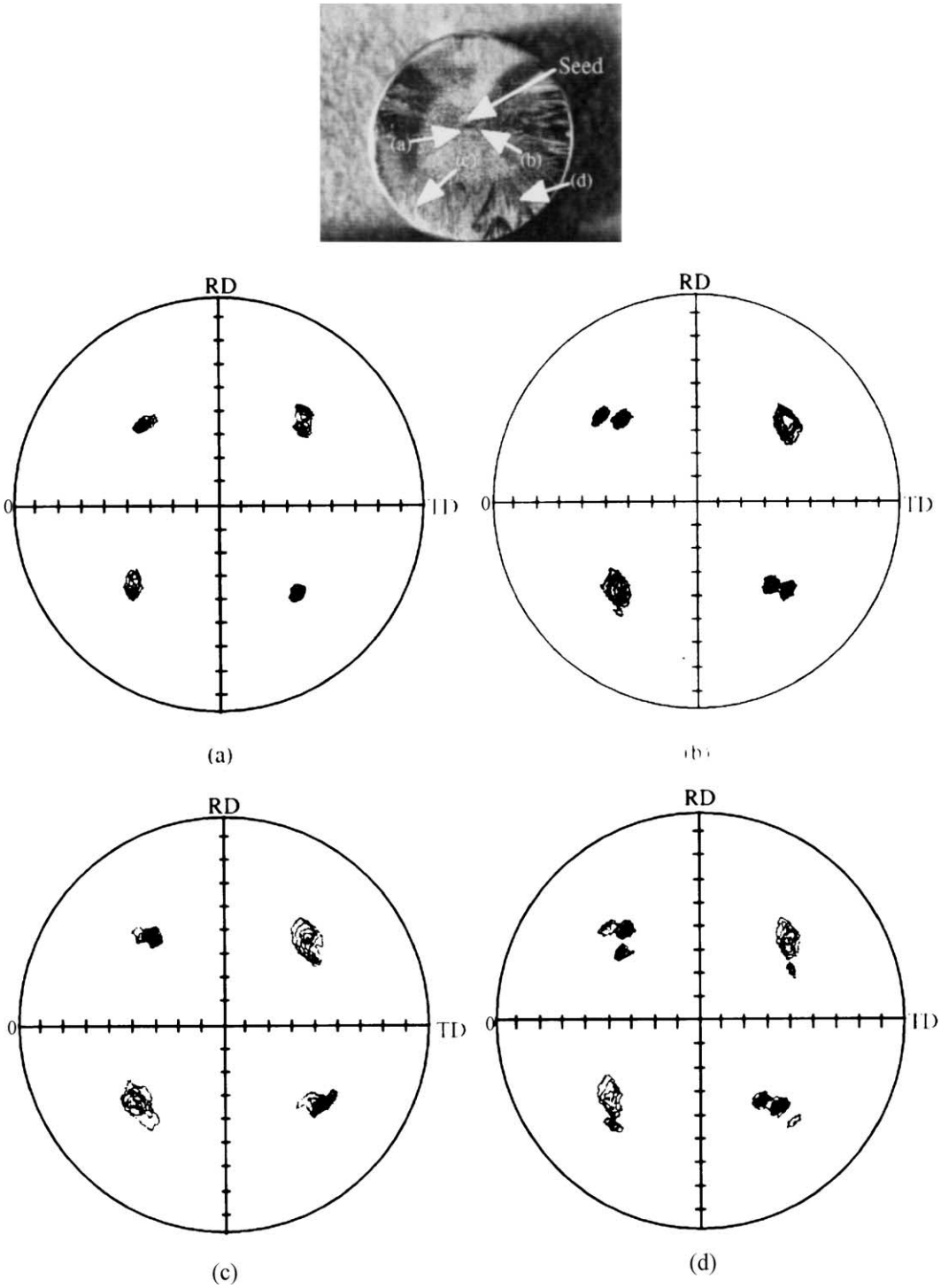

Fig. 5. Results of X-ray pole-figure analyses of (103) plane for sample A. The measured positions are presented in the inset. The positions (b) and (d) are near the area where the flux could easily penetrate, which was presented in Fig. 4(a) and (b).

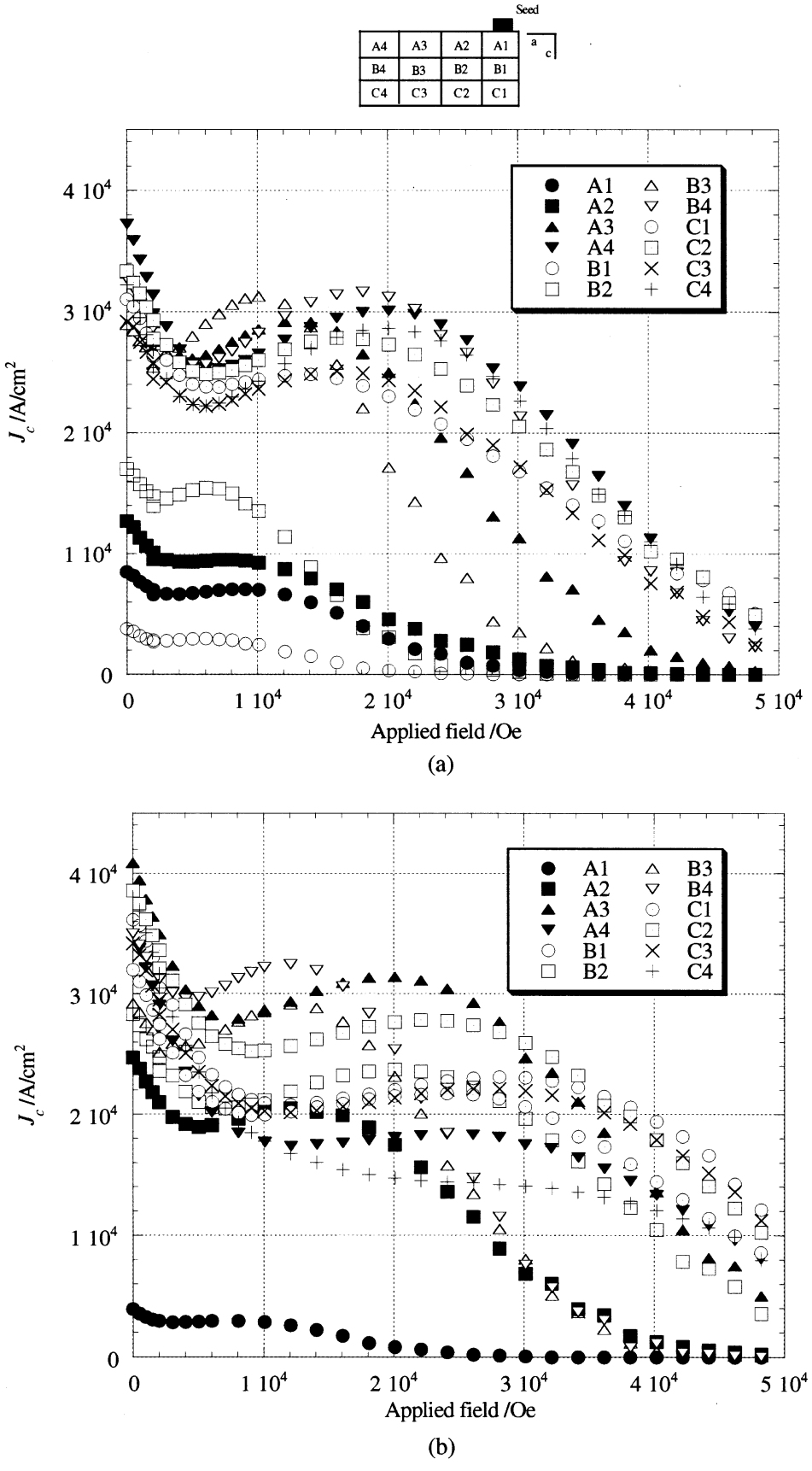

Fig. 6. J_c–B curves at 77 K for small specimens cut from various relative positions along a- and c-axis in samples (a) A and (b) B. The relative locations are presented in the inset.

superconducting quantum interference device magnetometer (SQUID) to determine the J_c values. Furthermore, X-ray pole-figure analyses were performed to measure the misorientation angles for sample A.

Next, we fabricated a bulk Nd–Ba–Cu–O sample with the same nominal composition of Nd123:Nd422 = 10:2 + 10 wt.%Ag_2O. The sample was also sintered in pure oxygen at 1040 °C for 1 h before the melt-growth. However, during the crystal growth, we changed the slow cooling rate from 1.0 to 0.3°C/h to crystallize this sample (sample C) to reveal the effect of cooling rate on the microstructure, the superconducting properties and the field-trapping capabilities. Except for the cooling rate, the heat schedules for this sample was the same as that for sample B (see Fig. 2).

We also prepared 10 wt.%Ag_2O-doped Nd–Ba–Cu–O bulk samples with different Nd422 content, Nd123:Nd422 = 10:1.5 (sample D), 10:2.5 (sample E) and 10:3 (sample F) to study the effect of Nd422 content on the microstructures, the superconducting properties, the field-trapping capabilities, and the mechanical properties. All the bulk samples were fabricated and oxygenated using the same thermal schedules shown in Fig. 2. We measured the trapped magnetic fields and maximum trapped-field values in liquid nitrogen using a Hall sensor. The field dependencies of the maximum trapped-field values were also measured. Small specimens were cut from samples D, E and F, and then DC magnetization measurements were carried out with a SQUID magnetometer to determine the J_c values. Microstructural observations at various locations were performed with a polarized microscope. Furthermore, the specimens for the tensile tests were cut from various

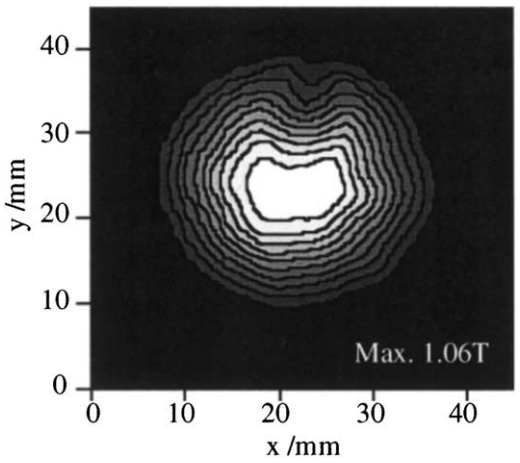

Fig. 7. Trapped-field distribution of sample C at liquid nitrogen temperature.

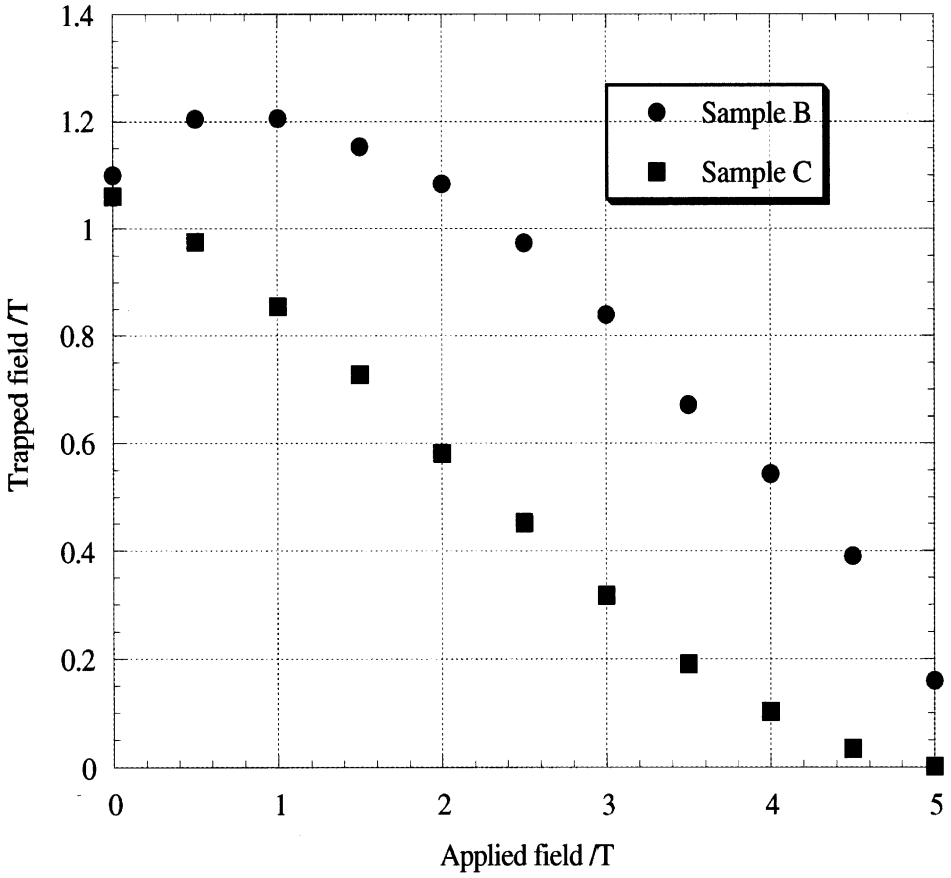

Fig. 8. Field dependencies of the maximum trapped-fields for samples B and C at liquid nitrogen temperature.

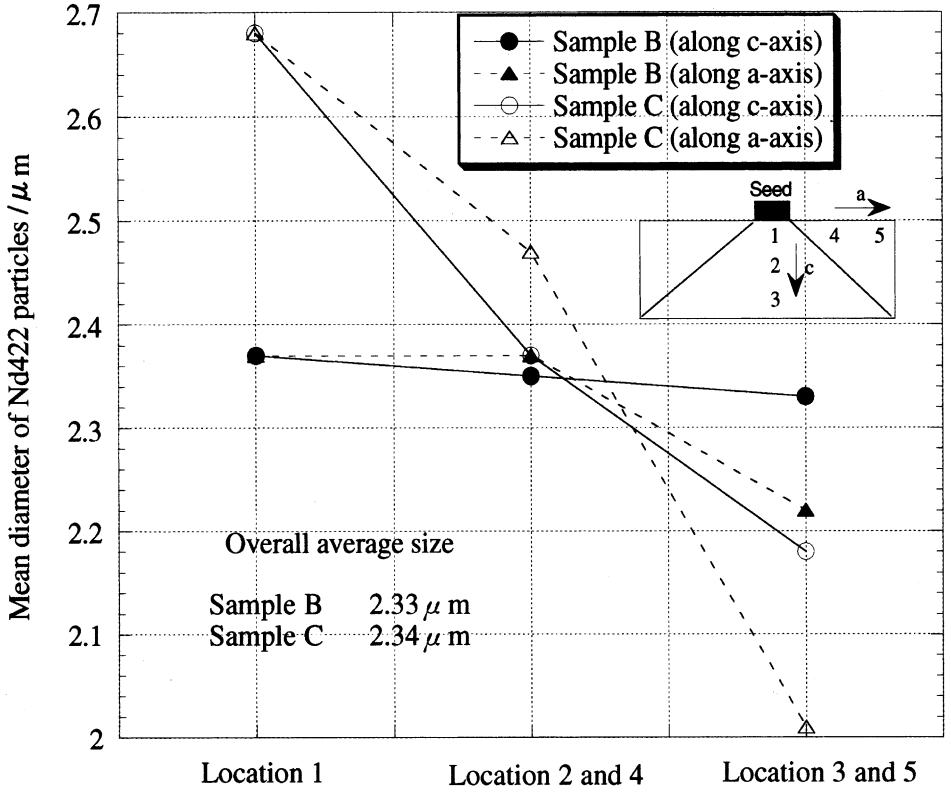

Fig. 9. Average sizes of Nd422 phase at various locations in samples B and C. The inset shows the analyzed locations.

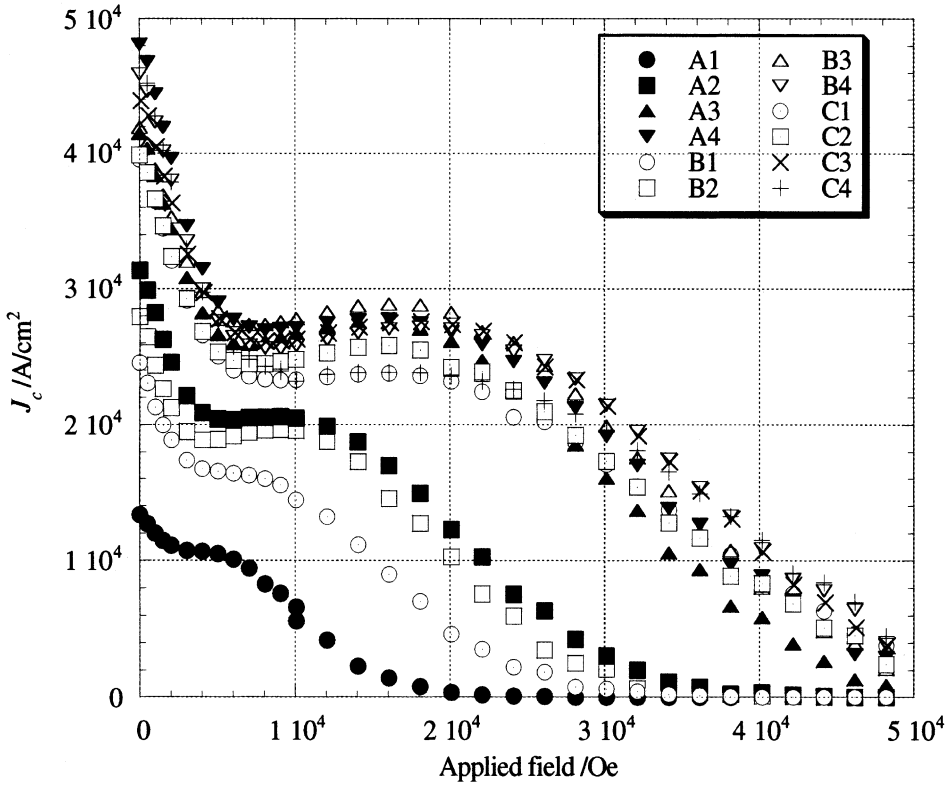

Fig. 10. Field dependencies of J_c values at 77 K for various locations in sample C. The relative locations are presented in the inset shown in Fig. 6(a).

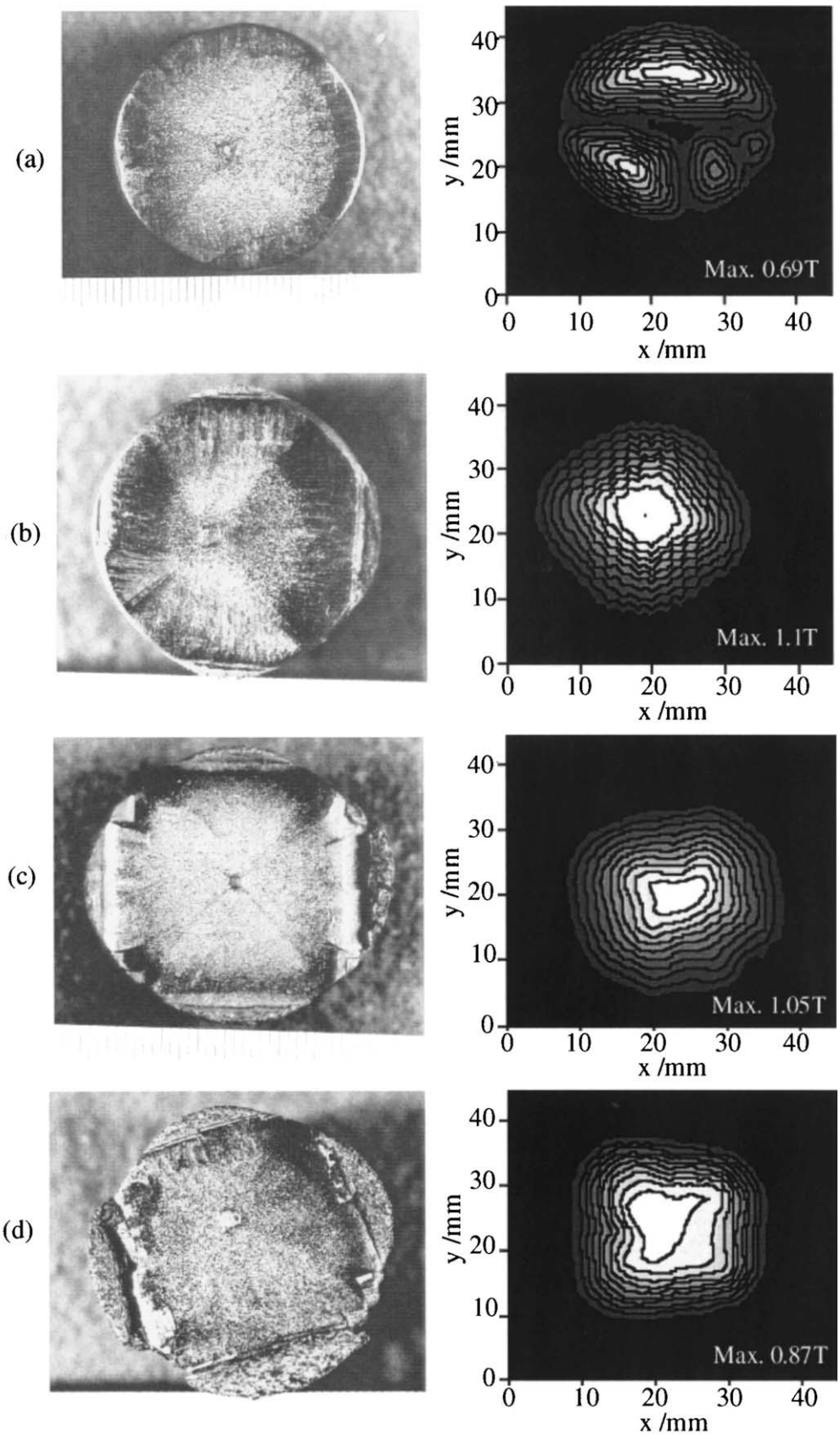

Fig. 11. Top views and field distributions trapped by 10 wt.%Ag_2O-doped Nd–Ba–Cu–O bulks with different Nd422 content at liquid nitrogen temperature: (a) Nd123:Nd422 = 10:1.5 (sample D), (b) 10: 2 (sample B), (c) 10:2.5 (sample E) and (d) 10:3 (sample F). The trapped-field distribution for sample B presented in Fig. 4(c) was again shown for comparison.

locations in samples B, D, E and F with dimensions of $3.5 \times 3.5 \times 12$ mm^3. The tensile loading direction was perpendicular to (100)/(010) plane of the specimens. The both edges of the specimens were covered with aluminum rods and firmly fixed with epoxy resin [20]. The rate of displacement for the tensile measurements was 0.5 mm/min.

In order to study the effect of Ag addition, we also fabricated the Nd–Ba–Cu–O bulk sample with the nominal composition of Nd123:Nd422 = 10:2 + 20 wt.%Ag_2O (sample G). The processing conditions for sample G were the same as those for sample B. After the trapped magnetic field in liquid nitrogen was measured, the maximum trapped-field value was monitored. The field dependence of the maximum trapped-field values was also measured. The tensile strength was measured like the tensile measurements of samples D, B, E and F.

Finally we fabricated the Nd–Ba–Cu–O bulk sample with the nominal composition of Nd123:Nd422 = 10:1.5 + 20 wt.%Ag_2O (sample H) to study the effect of Ag addition on the mechanical strength. The trapped-field distribution and the field dependence of the maximum trapped-field values were measured.

Since the trapped field values are known to depend on the sample thickness, we measured the trapped-field distribution and the maximum trapped-field value of the stacked samples by changing the thickness.

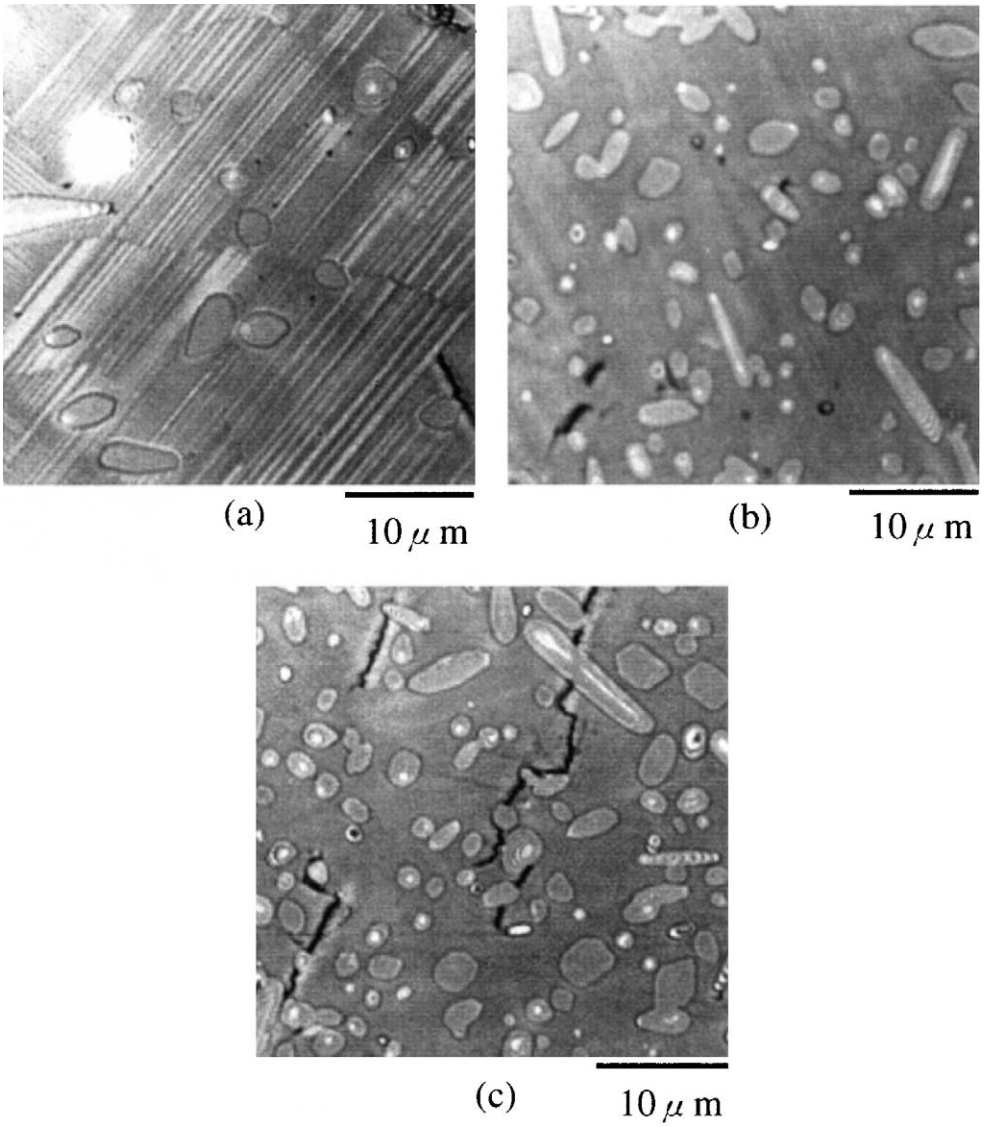

Fig. 12. (a–c) Optical micrographs and (d) the average sizes of Nd422 at the relative locations in samples D, B, E and F: (a) sample D (Nd123:Nd422 = 10:1.5 + 10 wt.%Ag_2O), sample B (Nd123:Nd422 = 10:2 + 10 wt.%Ag_2O), (b) sample E (Nd123:Nd422 = 10:2.5 + 10 wt.%Ag_2O) and (c) sample F (Nd123:Nd422 = 10:3 + 10 wt.%Ag_2O). The overall average sizes of Nd422 phase were 2.34, 2.33, 2.19 and 2.06 μm, respectively. The microstructure for sample B was already shown in Fig. 1(b).

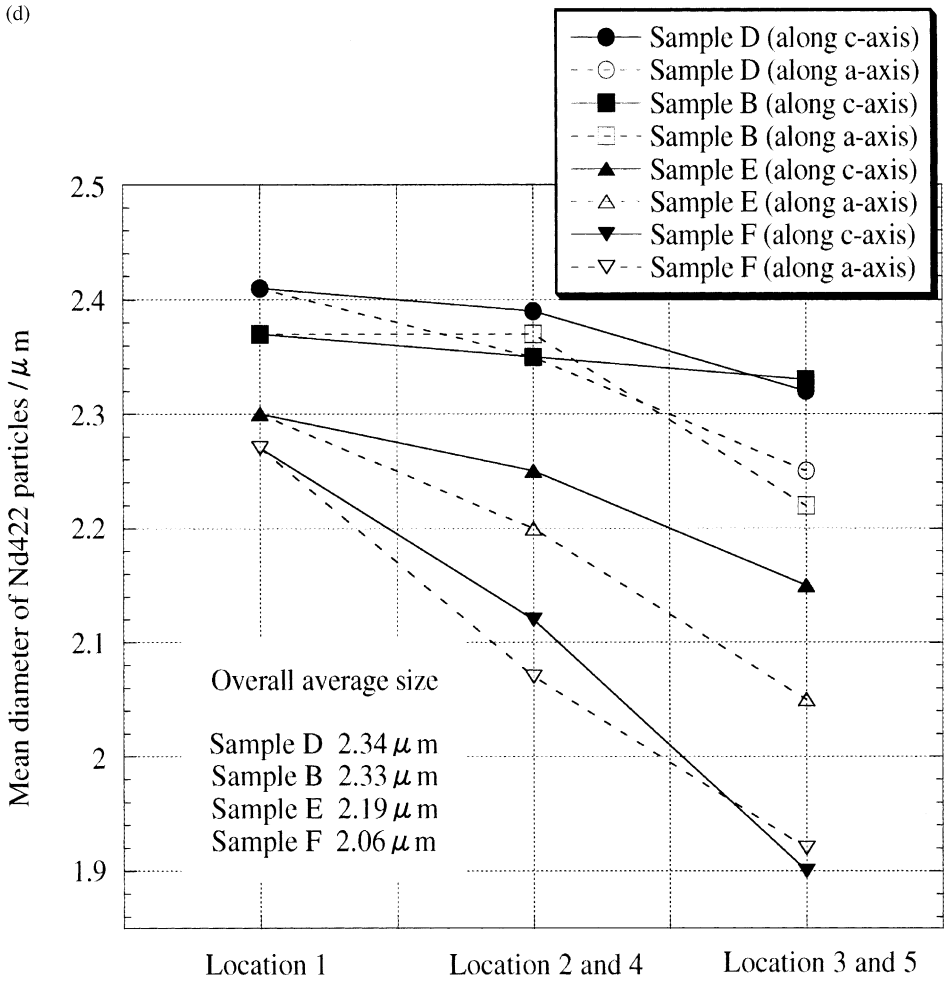

Fig. 12. (continued)

3. Results and discussion

3.1. Optimization of processing conditions

3.1.1. Pre-sintering effect before crystal growth

In this section, we investigated the effect of sintering before melt-processing on the superconducting properties and the field-trapping capabilities. The precursor powders with the composition of Nd123:Nd422 = 10:2 + 10 wt.%Ag_2O were used to fabricate single-domain Nd–Ba–Cu–O bulks. The density of the precursor pellet without sintering was only 4.5 g/cm^3, which was about 65% of the theoretical value of 6.96 g/cm^3. Due to such a low density, the samples were largely deformed after the melt-growth and a dent was formed near the center of the surface as shown in Fig. 3. The density of the pellet was increased to 6.5 g/cm^3 when sintered at 1040 °C for 1 h before the melt-growth. Such a precursor pellet with the high density was not deformed during the melt-process.

We also measured the densities of melt-grown crystals with and without pre-sintering treatment. The density of sample B with pre-sintering was 6.4 g/cm^3 and higher than that of sample A, 6.2 g/cm^3. This indicates that the pore density in sample A is larger than sample B, suggesting that more liquid loss occurred in sample A. Since a liquid loss during the melt-processing enhances the compositional shift toward Nd-rich direction, Nd-rich $Nd_{1+x}Ba_{2-x}Cu_3O_{7-\delta}$ has more tendency to form in sample A. However, even in sample B, the density decreased after the crystal growth presumably due to the generation of oxygen gas in a partially melted state, leading to the density lower than the theoretical value.

Fig. 4 shows the field distributions trapped by samples A and B in the remanent state, and the presence of 1T at liquid nitrogen temperature. Compared to sample B with symmetrical trapped-field distribution, sample A had the area where the flux could easily penetrate. In sample A, the flux already reached the center at 1T and the field distribution around the center was sectioned into two parts. This is partly attributed to the misorientation caused by the formation of subgrains, which was created by dislocation walls as a result of the entrapment of Nd422 particles in the matrix [21].

Fig. 5 shows the results of X-ray pole figure analyses for several positions on sample A. The positions (a) and

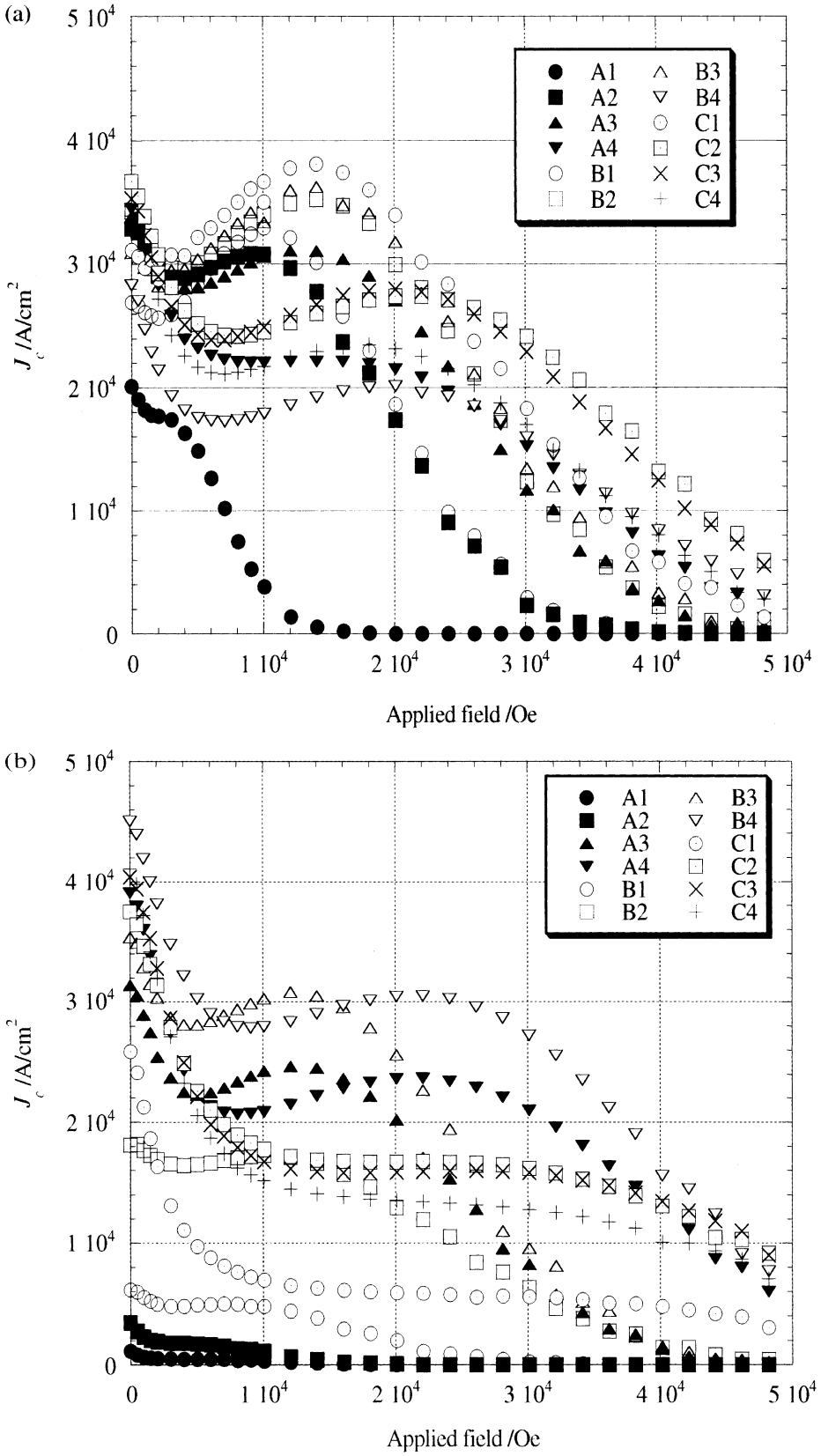

Fig. 13. Distributions of J_c–B properties at 77 K for the bulk samples with different Nd422 content: (a) sample D (Nd123:Nd422 = 10:1.5 + 10 wt.%Ag_2O), (b) sample E (Nd123:Nd422 = 10:2.5 + 10 wt.%Ag_2O) and (c) sample F (Nd123:Nd422 = 10:3 + 10 wt.%Ag_2O). The relative locations are presented in the inset shown in Fig. 6(a).

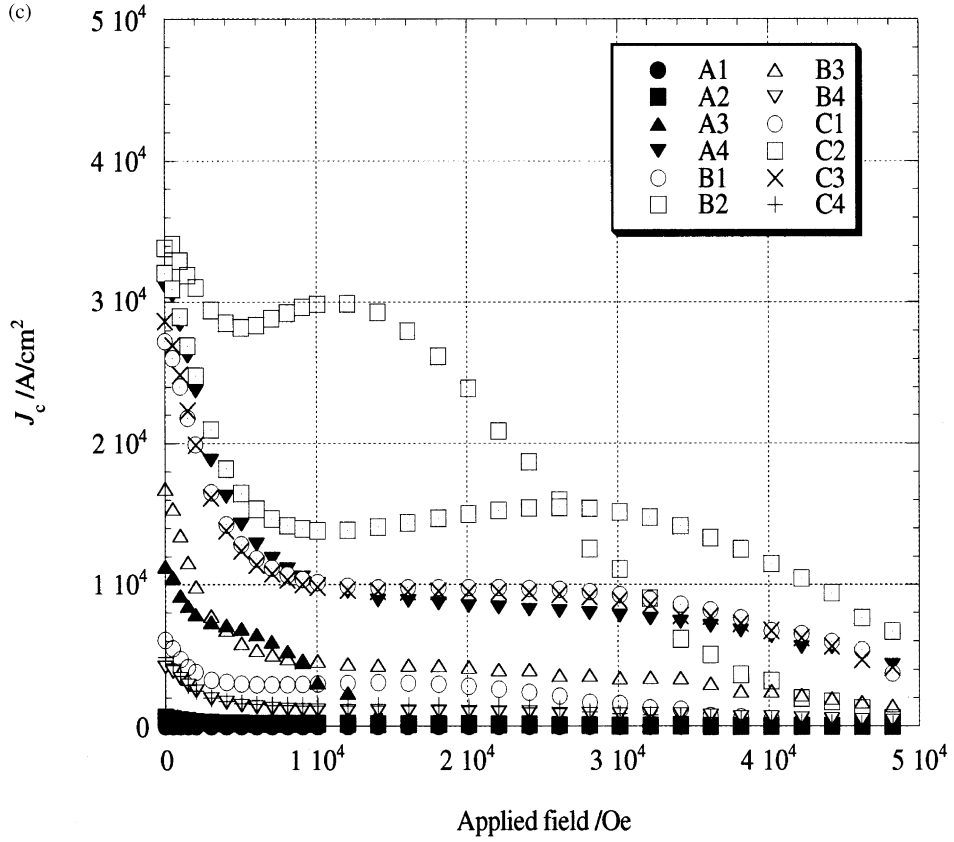

Fig. 13. (continued)

(b) are close to the seed, and the positions (c) and (d) are located near the periphery of sample A. Furthermore, the positions (b) and (d) are near the area where the flux could easily penetrate. It is evident that the misorientation angles between grains are larger in (c) and (d) than in (a) and (b). These results also support the idea that the misorientation is responsible for the weak-link behavior.

Fig. 6 shows J_c–B curves at 77 K for the small specimens cut from various positions along *a*- and *c*- axes in samples A and B. It is clear that J_c–B properties for sample A were more dispersive than those for sample B. Such inhomogeneity of J_c is attributed to a liquid loss caused by the lower density in sample A, which was not sintered before the crystal growth. It is also notable that the J_c values were very low at the locations beneath the seed in both samples A and B. This is attributed to the non-steady state solidification that took place at an early stage of crystallization [22], which may be the source of depressed superconducting properties caused by the large Nd/Ba substitution in Nd123 phase.

Considering the results of X-ray pole-figure analyses in Fig. 5 and the fact that the J_c values for sample A keep increasing from the center toward the edge, it is plausible that heavy deformation produced the area where the flux could easily penetrate.

For the fabrication of Nd bulk superconductors, it is very important to avoid a liquid loss and large deformation during the melt-processing. Sintering a sample prior to melt-processing was found to be effective in enhancing the superconducting properties and the field-trapping capability.

3.1.2. Effect of cooling rate during crystal growth

Nd–Ba–Cu–O bulk superconductors are sensitive to the processing conditions because the growth temperature [12] and the composition at the growth interface strongly affect the Nd/Ba substitution in Nd123 matrix. Hence, the cooling rate during the crystal growth is closely related to the Nd/Ba substitution. We investigated the effect of the cooling rate on the superconducting properties and the trapped-field values.

Fig. 7 shows the trapped-field distribution of sample C at liquid nitrogen temperature. The field distribution trapped by sample B was already presented in Fig. 4(c). Both samples had the trapped-fields higher than 1T. It is evident that a decrease in the growth rate from 1.0 to 0.3 °C/h did not degrade the field-trapping capability in the remanent state. Fig. 8, however, shows a clear difference between sample B and sample C in that the maximum trapped-field values are plotted as a function of the external field. The trapped-field values of sample B are always higher than those of sample C. It is also notable that the secondary peak effect is observed in sample B, while it is absent in sample C.

The trapped-field is correlated with the microstructures and the average J_c–B properties in the entire sample. Therefore, homogeneous microstructures and J_c–B properties are important for achieving a high field-trapping capability. In sample C, the grain size of Nd422 inclusions in the matrix was strongly dependent on the distance from the seed due to the pushing effect of Nd422 particles. As shown in Fig. 9, the size decreased with distance from the seed both in the horizontal and vertical directions. In contrast, the size distribution in sample B was smaller than that in sample C. These features are closely related to the amount of undercooling (ΔT), where ΔT is the difference between T_p and the growth temperature [23]. It is well known that small particles can be trapped by the matrix as ΔT becomes large. Therefore, in sample C fabricated at the slower cooling rate of 0.3 °C/h, the distribution of Nd422 inclusions is less homogeneous and smaller Nd422 particles were entrapped in a large ΔT region far away from the seed. Such microstructural variation within the sample causes the location dependence of J_c–B properties because the average size of non-superconducting particles affects the remanent J_c value and furthermore the pushing/trapping behavior of Nd422 changes the composition at the growth front. Besides this, the Nd/Ba chemical fluctuation is also dependent on the growth temperature and ΔT, which also affects the superconducting properties. Fig. 10 shows the field dependencies of J_c values for various locations in sample C. Apart from the region beneath the seed (region A1) with the lowest J_c values due to non-steady solidification discussed in Section 3.1 [22], it is clear that sample B contains the regions exhibiting remarkable secondary peak effect with the relatively high peak field while some regions are observed in sample C, where the J_c–B properties are gradually improved with the distance from the seed. This is due to the fact that the range of Nd/Ba substitution depends on the undercooling, the mass valance in the bulks and the pushing/trapping behavior of Nd422 at the growth interface. In the case of the cooling rate of 0.3 °C/h, the crystal began to grow under the smaller ΔT and hence the crystal solidified at the early stage had the smaller Nd/Ba substitution in the matrix. This substitution becomes large with increasing ΔT [12] until it is suppressed by the mass valance. Furthermore, the amount of pushed Nd422 particles is larger, which tends to generate Nd-rich Nd123 phase. Accordingly, the area where Nd123ss phase with the relatively large Nd/Ba substitution was enlarged compared with sample B.

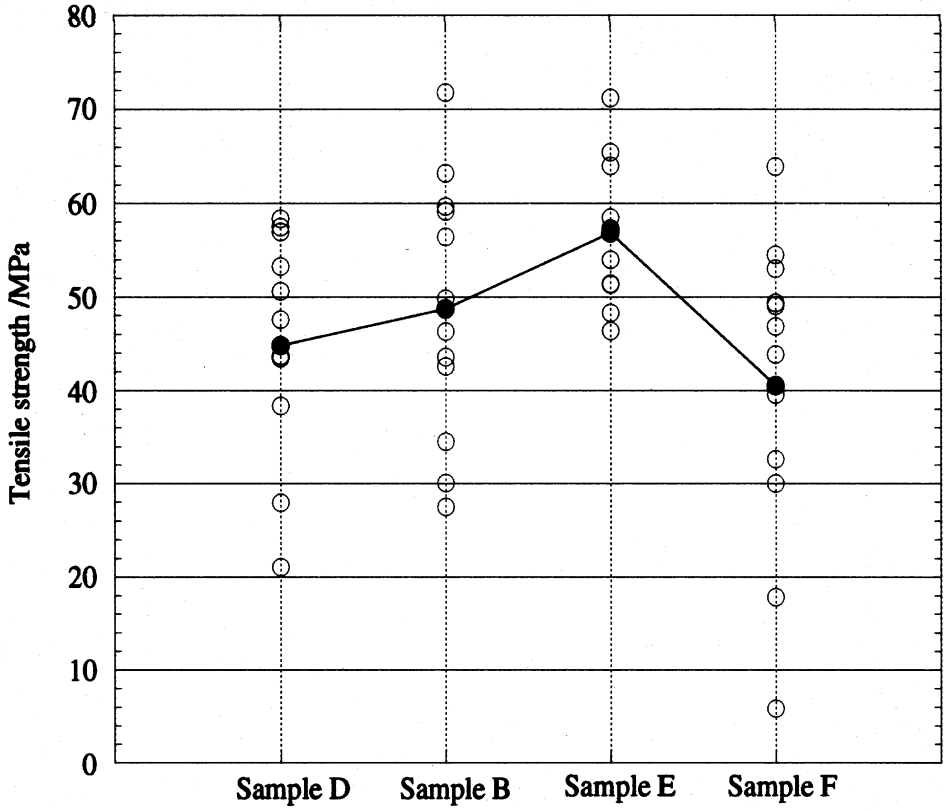

Fig. 14. Tensile strengths of the specimens cut from the various locations in the grown samples with different Nd422 content: sample D (Nd123:Nd422 = 10:1.5 + 10 wt.%Ag_2O), sample B (Nd123:Nd422 = 10:2 + 10 wt.%Ag_2O), sample E (Nd123:Nd422 = 10:2.5 + 10 wt.%Ag_2O) and sample F (Nd123:Nd422 = 10:3 + 10 wt.%Ag_2O).

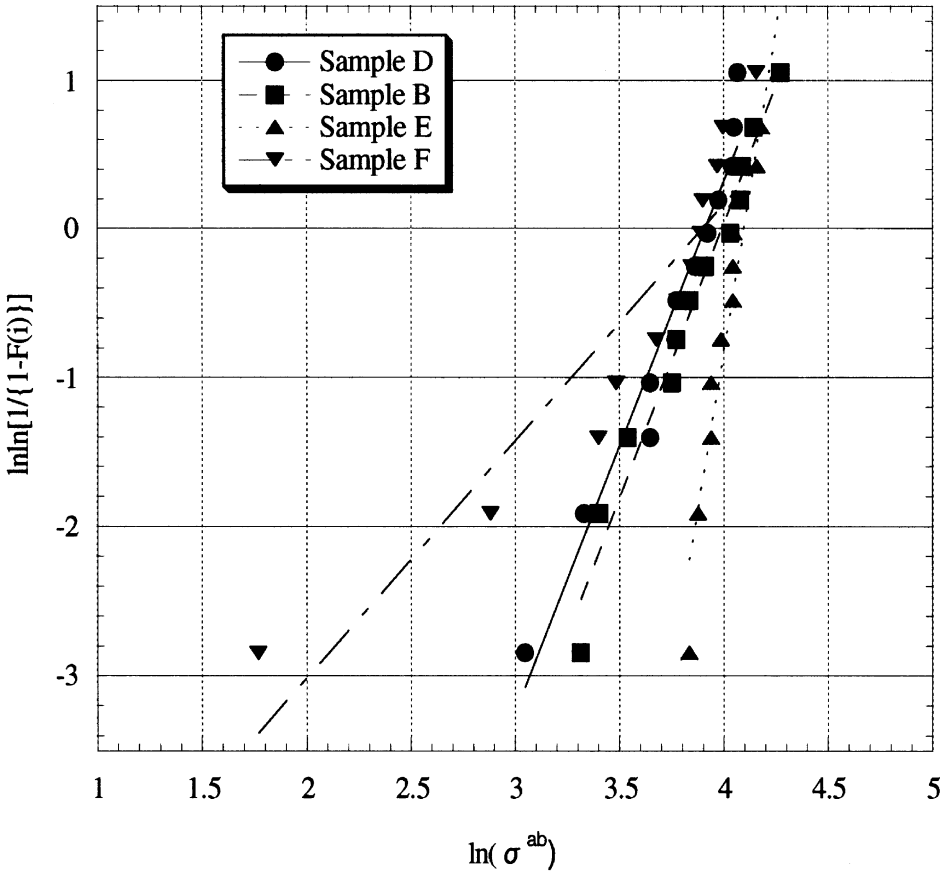

Fig. 15. Weibull plots of tensile strengths for the bulk samples with different Nd422 content: sample D (Nd123:Nd422 = 10:1.5 + 10 wt.%Ag_2O), sample B (Nd123:Nd422 = 10:2 + 10 wt.%Ag_2O), sample E (Nd123:Nd422 = 10:2.5 + 10 wt.%Ag_2O) and sample F (Nd123:Nd422 = 10:3 + 10 wt.%Ag_2O). The Weibull coefficients of samples D, B, E and F are 3.56, 3.68, 8.61 and 1.59, respectively.

Considering the correlation with the trapped-fields already presented in Fig. 7 and the J_c–B properties, the average J_c–B properties in the entire samples reflected the trapped-fields and therefore the peak effect of sample C in the trapped-field as a function of the external field was smeared out in the course of integration of J_c values. Consequently, we must pay particular attention to the pushing/trapping behavior of Nd422 and the growth temperature, which strongly affect the Nd/Ba substitution in Nd123 matrix at the growth interface, in order to achieve a superior field-trapping ability in the Nd–Ba–Cu–O system. Furthermore, the present results in this section suggest that for the characterization of large grain materials, the measurement of the trapped-field in the remanent state is not sufficient to fully characterize the materials properties. In Nd system, although the trapped-field value was almost the same for large grain materials crystallized at different cooling rates, both the J_c–B properties and the field dependence of the trapped-field were different. In this particular system, a relatively larger growth rate provided better superconducting properties along with more uniform microstructure.

3.2. Effect of Nd422 and Ag content for the field-trapping capability and the mechanical properties

3.2.1. Effect of Nd422 content on the field-trapping capability and the mechanical properties

In this section, we investigated the effect of Nd422 content on the microstructures, the superconducting properties and the field-trapping capabilities for Nd bulk samples.

Fig. 11 shows the top views and the field distributions trapped by 10 wt.%Ag_2O-doped Nd bulks with different Nd422 content:Nd123:Nd422 = 10: 1.5 (sample D), 10: 2 (sample B presented in Fig. 3), 10:2.5 (sample E) and 10:3 (sample F). It is evident that the segregation of Nd422 particles at the periphery of a bulk increased with increasing Nd422 content, related to the magnitude of undercooling. Fig. 12 shows the microstructures and the average grain sizes of Nd422 particles at relative locations in the bulks. The amount of Nd422 particles trapped in the matrix increased with Nd422 content. An excessive addition of Nd422 caused the segregation of Nd422, leading to inhomogeneous microstructure in the bulk. As the distance from the seed increases, the

amount of Nd422 trapped in the matrix increased accompanied by the size reduction of Nd422. Furthermore, the composition at the growth front tends to shift toward Nd-rich direction with increasing the amount of Nd422 inclusions pushed away from the growth interface and hence the Nd/Ba substitution is enhanced in the matrix, which resulted in poor superconducting properties. In order to confirm this fact, we measured the field dependencies of J_c values at various locations in the bulk samples. Fig. 13 shows the distributions of J_c–B properties for the samples with different Nd422 content. The J_c–B properties for the sample with the nominal composition of Nd123: Nd422 = 10:2 + 10 wt.%Ag_2O (sample B) are already presented in Fig. 6(b).

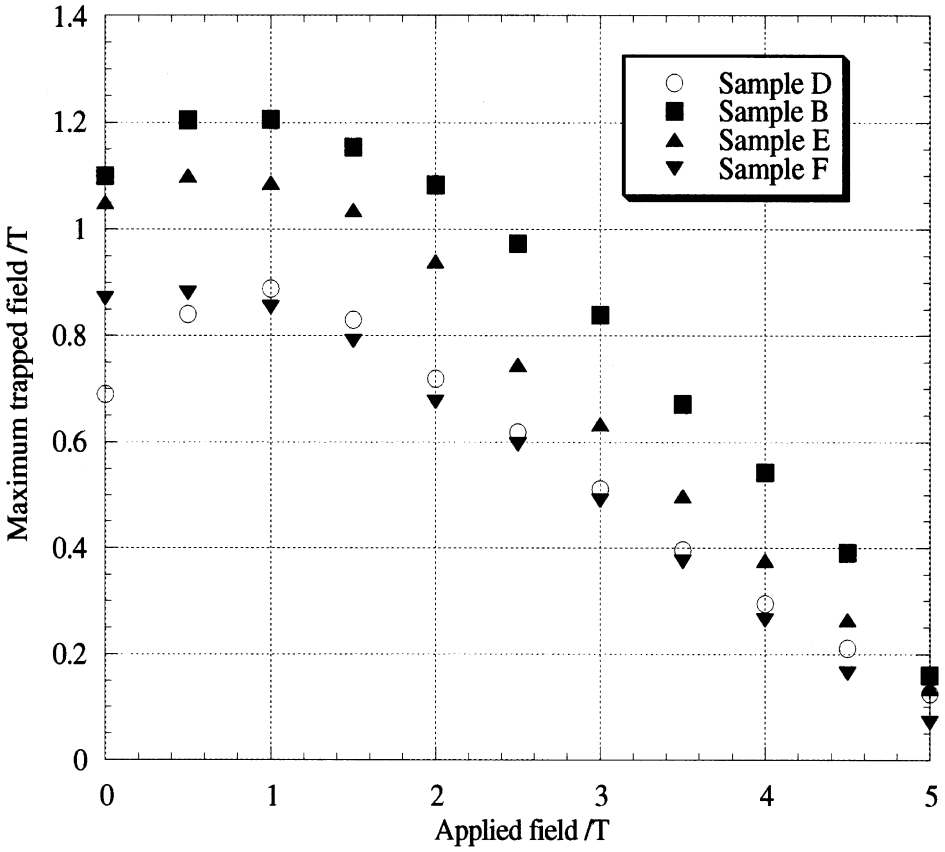

Fig. 16. The maximum field values trapped by Nd bulk superconductors with different Nd422 content as a function of the external field at liquid nitrogen temperature: sample D (Nd123:Nd422 = 10:1.5 + 10 wt.%Ag_2O), sample B (Nd123:Nd422 = 10:2 + 10 wt.%Ag_2O), sample E (Nd123:Nd422 = 10:2.5 + 10 wt.%Ag_2O) and sample F (Nd123:Nd422 = 10:3 + 10 wt.%Ag_2O). Sample D contained some large-size cracks, representing the maximum trapped-field values as open symbols.

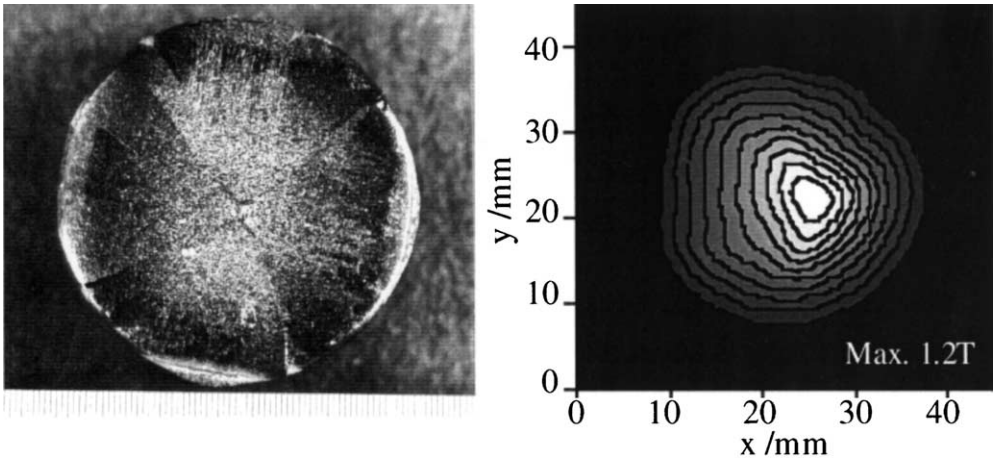

Fig. 17. Top view and trapped-field distribution of sample G (Nd123:Nd422 = 10:2 + 20wt.%Ag_2O) at liquid nitrogen temperature.

The more homogeneous J_c–B properties could be obtained with decreasing Nd422 content presumably because the amount of Nd422 particles pushed from the growth front decreased. Furthermore, the prominent peak effect was observed in sample D with the smallest Nd422 content. This is understandable by considering the fact that the peak effect originates from the chemical variation in the matrix and therefore the sample with the largest volume of Nd123 matrix exhibited the remarkable peak effect. As a result, the trapped-field distributions of Nd bulks with the larger amount of Nd422 particles were less symmetrical. Unfortunately, single-domain bulk sample with the composition of Nd123:Nd422 = 10:1.5 + 10 wt.%Ag_2O contained large-size cracks even though we could fabricate single-domain samples for all the compositions, suggesting that Nd422 particles affected the mechanical properties of a bulk sample. Fig. 14 shows the tensile strengths of the rectangular specimens cut from the various locations in the grown samples with different Nd422 content. A gradual increase of the average tensile strength was observed, and the sample with the initial composition of Nd123:Nd422 = 10:2.5 exhibited the average tensile strength of 56.8 MPa. It is notable that the minimum tensile strength was largely improved with increasing Nd422 content up to the composition of Nd123:Nd422 = 10:2.5. A further Nd422 addition increased the scattering of the tensile strengths and thus decreased the average tensile strength. Accordingly, the main contribution of Nd422 particles to the mechanical properties was an increase in the lowest tensile strength, leading to the homogeneous distribution of the mechanical properties. In our experiments, the overall average sizes of Nd422 particles for all the samples were larger than 2 μm as already presented in Fig. 12. Furthermore, a bulk superconductor has crystallographic features, e.g. microcracks and porosity that strongly affect the mechanical properties. Therefore, Nd422 particles dispersed in the matrix did not contribute to particulate reinforcement but suppressed the propagation of cracking. For engineering applications, the reliability of mechanical strength is very important. The Weibull distribution function $F(\sigma)$ is often used to evaluate this reliability. $F(\sigma)$ is expressed as follows [24]:

$$F(\sigma) = 1 - \exp\left[-\left(\frac{\sigma}{\sigma_0}\right)^m\right] \quad (1)$$

where σ is the tensile strength, m is the Weibull coefficient and σ_0 is a constant. Generally, $F(\sigma)$ is evaluated in the following logarithmic form:

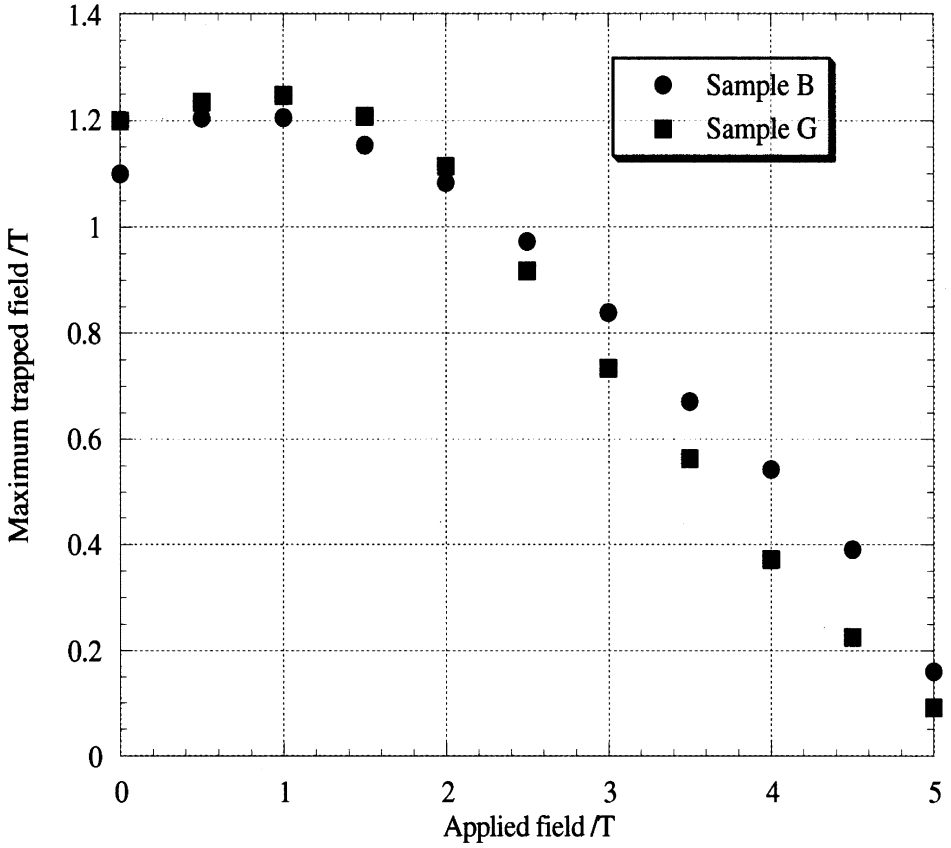

Fig. 18. Field dependencies of the maximum trapped-fields for sample B (Nd123:Nd422 = 10:2 + 10 wt.%Ag_2O) and sample G (Nd123:Nd422 = 10:2 + 20 wt.%Ag_2O) at liquid nitrogen temperature.

$$\ln\ln\left(\frac{1}{1-F(\sigma)}\right) = m\ln\sigma - m\ln\sigma_0 \quad (2)$$

For convenience, $F(i)$ is approximated by

$$F(i) = \frac{(i-0.3)}{(n+0.4)} \quad (3)$$

where i is the order of destruction and n is the number of samples. Fig. 15 shows the Weibull plots of tensile strengths for the bulk samples with different Nd422 content. The Weibull coefficient was largely enhanced with increasing Nd422 content up to ratio of 2.5. It should be noted that the sample with the composition of Nd123: Nd422 = 10: 2.5 exhibited very high Weibull coefficient exceeding 8. The Weibull coefficient decreased with further addition of Nd422. This result also suggests that appropriate Nd422 addition is required to make the more uniform distribution of mechanical strength. Fig. 16 shows the maximum field values trapped by Nd bulk superconductors with different Nd422 content as a function of the external field. Except for sample D containing large-size cracks, since the higher trapped-field values were achieved in the sample with large secondary peak effect, it is probable that the higher trapped-field value can be obtained if the sample without large-size cracks is fabricated in the initial composition of Nd123:Nd422 = 10:1.5. According to previous reports [15–17], Ag addition improved the mechanical properties, however, the function of Ag particles was not discussed in detail. Hence, we investigated the effect of Ag addition on the microstructures, the superconducting properties, the field-trapping capability and the mechanical properties.

3.2.2. Effect of Ag addition on the field-trapping capability and the mechanical properties

In this section, we investigated the effect of Ag_2O content on the field-trapping capabilities and the mechanical properties. Fig. 17 shows the top view and the trapped-field distribution of sample G (Nd123:Nd422 = 10:2 + 20 wt.%Ag_2O). One can see that a single grain can be grown even with this amount of Ag.

Fig. 18 shows the field dependencies of the maximum trapped-fields for samples B and G. Their field dependencies were very similar because there was no appreciable difference in the microstructures and the superconducting properties for these samples. Thus, it is concluded that an increase in Ag content from 10 to 20 wt.% did not affect the field-trapping ability.

However, the distribution of mechanical properties was quite different. Fig. 19 shows the tensile strengths of

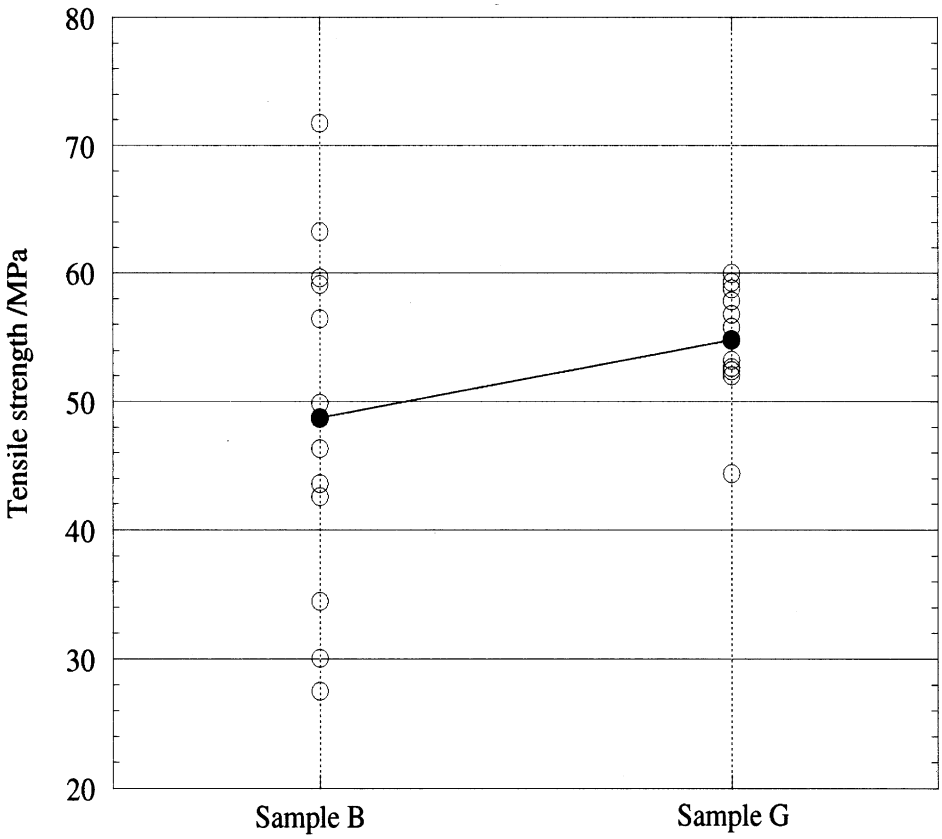

Fig. 19. Tensile strengths of the specimens cut from sample G (Nd123:Nd422 = 10:2 + 20 wt.%Ag_2O). The tensile strengths for the specimens cut from sample B (Nd123:Nd422 = 10:2 + 10 wt.%Ag_2O) were also depicted for comparison.

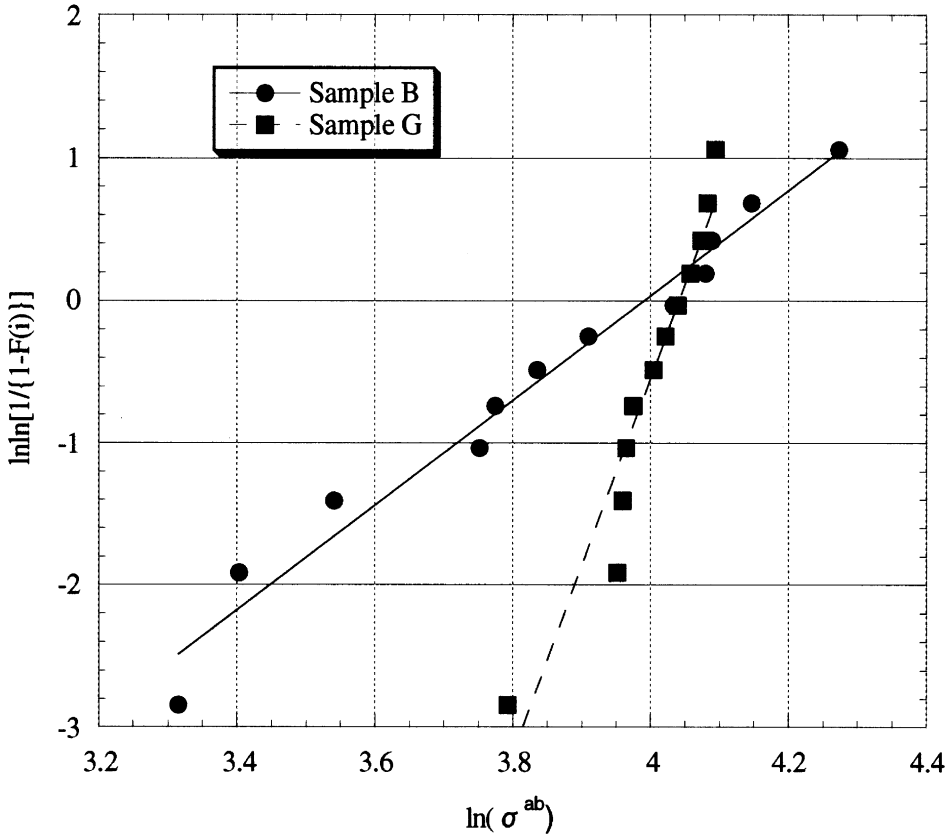

Fig. 20. Weibull plots of tensile strengths for the bulk samples with different Ag_2O content: sample B (Nd123:Nd422 = 10:2 + 10 wt.%Ag_2O) and sample G (Nd123:Nd422 = 10:2 + 20 wt.%Ag_2O). The Weibull coefficient increased from 3.68 to 13.18 with further Ag_2O addition.

the specimens cut from sample G. Here, the tensile strength values for sample B are also plotted in Fig. 19 in comparison with the values for sample G. Besides some improvement of the average tensile strength, the scattering of the tensile strength values in sample G drastically decreased and also the Weibull coefficient exceeded 13 as shown in Fig. 20. For practical applications, the materials should have the Weibull coefficient higher than 5 [20]. Hence sample G is a desirable engineering material from viewpoints of the mechanical properties. Furthermore, Ag particles functioned as barriers against cracking like Nd422 inclusions. This is deduced by the fact that the average tensile strength value increased with Ag addition. One can also observe that large-size cracks introduced from pores are blunted by Ag particles as shown in Fig. 21. Some crack propagation also stopped at Ag particles. This also supports the idea that Ag particles contribute to crack blunting.

Fig. 22 shows the top view and the trapped-field distribution of the sample H with the nominal composition of Nd123:Nd422 = 10:1.5 + 20 wt.%Ag_2O. One can see that a single-domain with no macrocracks could be obtained, which contrasts with the results of sample D with 10 wt.%Ag_2O which contained several large-size cracks (see Fig. 11). It is evident this is due to the beneficial effect of Ag particles on mechanical properties. Fig. 23 shows the field dependence of the trapped field for sample H. A remarkable secondary peak effect is observed. It is also notable that the maximum trapped-field value reached 1.4T in the remanent state, and even a larger value of 1.6T in the presence of 1T at 77 K.

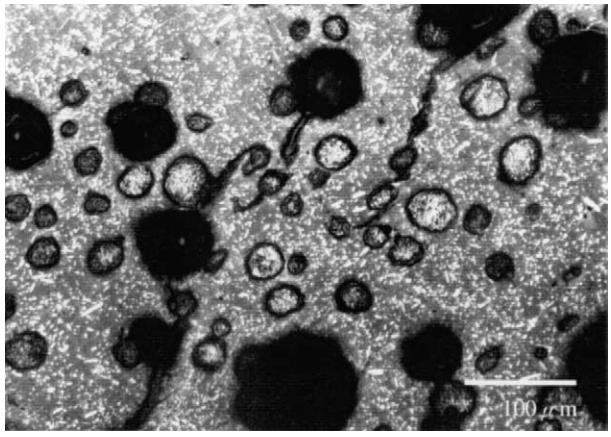

Fig. 21. Large-size cracks introduced from pores are blunted or stopped by Ag particles. The observed position was close to the fractured surface of a specimen. Large black regions are pores. Large white and gray particles are Ag particles. Small white particles in the matrix are Nd422 particles.

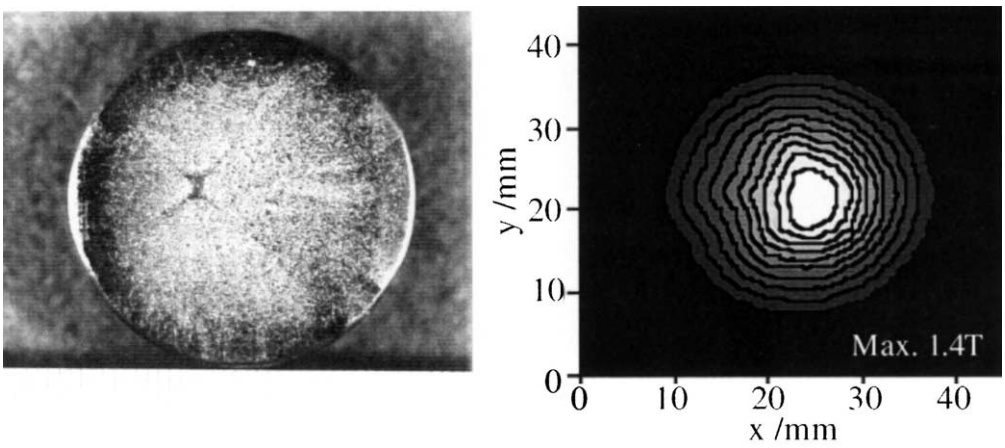

Fig. 22. Top view and the field distribution trapped by sample H (Nd123:Nd422 = 10:1.5 + 20 wt.%Ag_2O) at liquid nitrogen temperature.

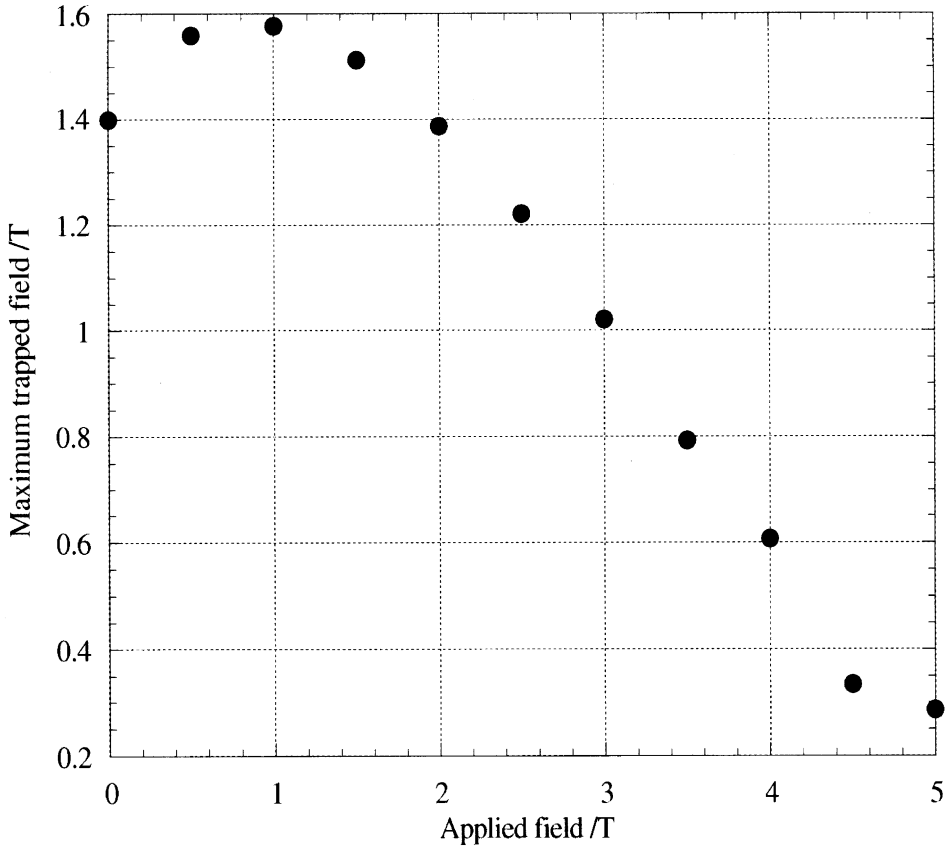

Fig. 23. Field dependence of the maximum trapped-field for sample H (Nd123:Nd422 = 10:1.5 + 20 wt.%Ag_2O) at liquid nitrogen temperature.

These results show that the optimization of processing conditions and the content of Nd422 and Ag_2O lead to the production of a good quality Nd–Ba–Cu–O large-grain sample with the trapped-field exceeding 1T at 77K along with a high reliability of the mechanical strength.

3.3. Higher trapped-field for future engineering

The demagnetizing effect has always a negative influence on the trapped-field value of bulk superconductors in practical dimensions. Hence, for fair comparison it is necessary to minimize the demagnetizing effect by increasing the thickness of the sample. The effective thickness of a bulk superconductor can be increased simply by stacking different blocks.

Fig. 24 shows the remnant trapped-field distribution when the three samples are stacked. The data of 1.4T plotted at 10 mm thickness is the one for sample H. Then we stacked the sample about 5 mm in thickness, and the trapped-field was increased to 1.6T. This is due

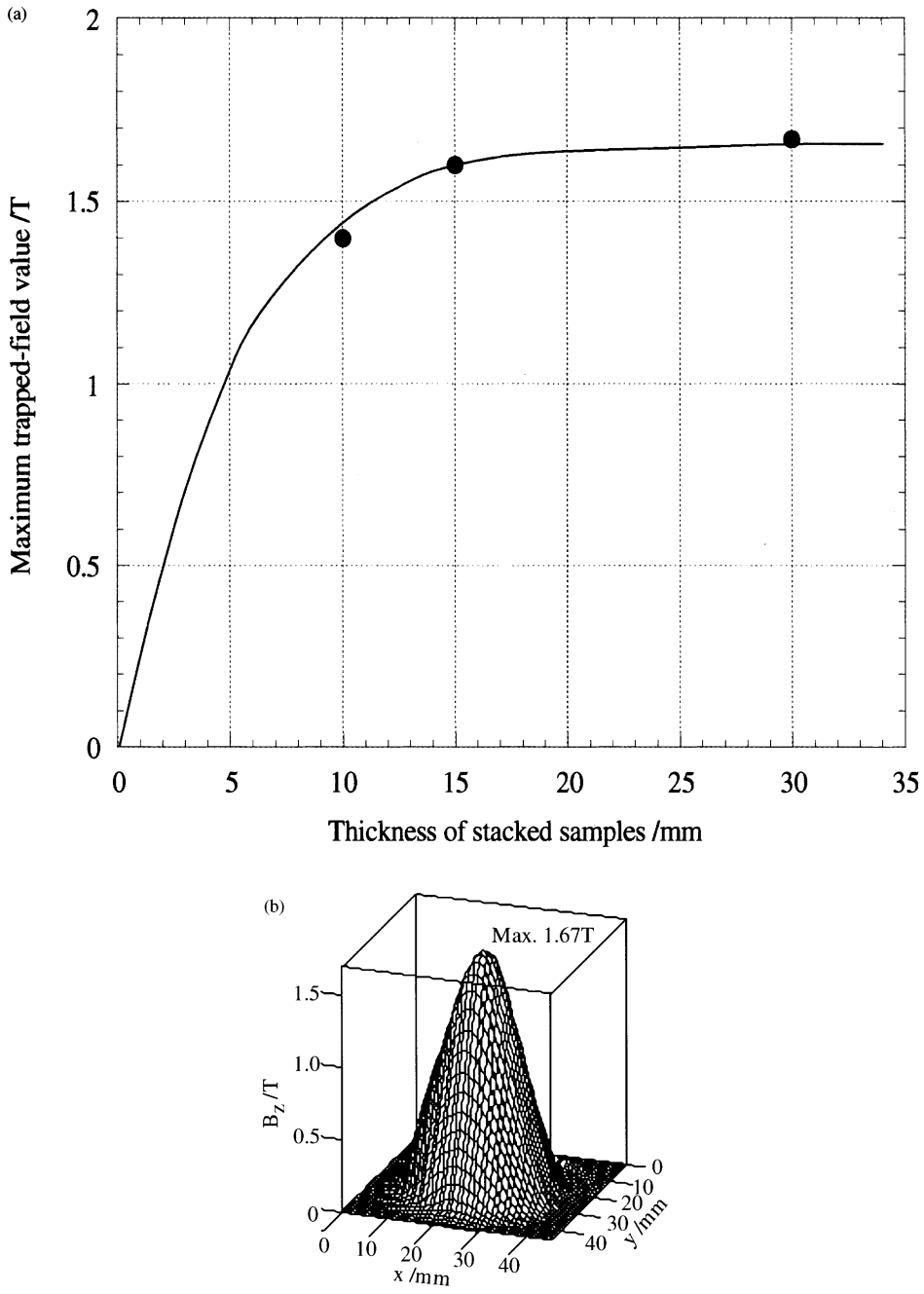

Fig. 24. (a) The maximum trapped-field values as a function of the thickness of stacked samples at liquid nitrogen temperature. The effective thickness of samples was changed by stacking the different bulks. The top sample was sample H with the trapped-field of 1.4T in the remanent field at 77 K. (b) The field distribution trapped by stacked samples 30 mm in total thickness in the remanent field.

to a reduction in the demagnetizing effect. The trapped-field value was slightly enhanced to 1.67T at 77 K where th > e total thickness was 30 mm, but an increase was very small. It has been reported that the trapped-field can be increased by increasing the thickness, but saturates at a certain thickness [25]. Our results can be understood in terms of the saturation of the trapped-field. These results show that this sample has an ability to trap 1.67T at 77 K.

4. Conclusions

Nd–Ba–Cu–O bulk superconductors were fabricated with different initial compositions under different processing conditions in 1%O_2-Ar atmosphere in order to improve the field-trapping capability and the mechanical properties. Low density samples suffered from a large deformation during processing and the areas where the flux could easily penetrate. Such a problem

could be overcome by sintering a sample before the crystal growth. With this treatment, we could also reduce a liquid loss causing the composition shift toward the Nd-rich direction in Nd123 phase. Furthermore, the Nd/Ba substitution ratio in Nd123 phase is closely related to the growth temperature, the composition at the growth interface and the mass valance in a bulk. A relatively large cooling rate during the crystal growth and smaller Nd422 addition suppressed the volume in which Nd substitutes on Ba site, resulting in a more symmetrical trapped-field distribution with the enhancement of the maximum trapped-field value.

For the achievement of homogeneous mechanical properties, an addition of appropriate amount of Nd422 and Ag was required. Nd422 and Ag particles could suppress crack propagation, leading to the improvement of the minimum mechanical strength. These normal conducting inclusions however did not contribute to particulate reinforcement of a bulk sample because their average size was too large.

As a result of optimized processing conditions, we could obtain the bulk sample exhibiting a trapped-field of 1.4T in the remnant state at 77 K. The same sample could trap 1.6T in the presence of 1T due to the prominent fishtail effect. The trapped field in the remanent state increased to 1.67T when the field was monitored on the surface of stacked samples 30 mm in thickness. Furthermore, optimally processed bulk samples showed a high reliability in the mechanical strength, where the Weibull coefficient and the average tensile strength exceeded 13 and 50 MPa.

Acknowledgements

The author is grateful to Dr. Sakai, Dr. Nariki and Dr. Ogasawara for fruitful discussions. This work was supported by the New Energy and Industrial Technology Development Organization (NEDO) as Collaborative Research and Development of Fundamental Technologies for Superconductivity Applications.

References

[1] K. Salama, V. Selvamanickam, L. Gao, K. Sun, Appl. Phys. Lett. 54 (1989) 2352–2354.
[2] M. Murakami, M. Morita, K. Doi, K. Miyamoto, Jpn. J. Appl. Phys. 28 (1989) 1189–1194.
[3] M. Matsui, N. Sakai, S. Nariki, S.J. Seo, M. Murakami, Supercond. Sci. Technol. 13 (2000) 660–664.
[4] I. Monot, J. Wang, M.P. Delamare, S. Marinel, M. Hervieu, J. Provost, G. Desgardin, Physica C 282–287 (1997) 507–508.
[5] S. Nariki, N. Sakai, M. Murakami, Physica C 357 (2001) 811–813.
[6] M. Muralidhar, M.R. Koblischca, P. Diko, M. Murakami, Appl. Phys. Lett. 76 (2000) 91–93.
[7] D.G. Hinks, L. Soderholm, D.W. Capone II, J.D. Jorgensen, I.K. Schuller, C.U. Segre, K. Zhang, J.D. Grace, Appl. Phys. Lett. 50 (1987) 1688–1690.
[8] M. Murakami, Appl. Supercond. 6 (1998) 51–59.
[9] S.I. Yoo, R.W. McCallum, Physica C 210 (1993) 147–156.
[10] K. Takita, H. Katoh, H. Akinaga, M. Nishino, T. Ishigaki, H. Asano, Jpn. J. Appl. Phys. 27 (1988) 57–60.
[11] S.I. Yoo, N. Sakai, H. Takaichi, T. Higuchi, M. Murakami, Appl. Phys. Lett. 65 (1994) 633–635.
[12] K. Osamura, W. Zhang, Z. Metallkd 84 (1993) 522–529.
[13] Y. Ren, R. Weinstein, J. Liu, R.P. Sawh, C. Foster, Physica C 251 (1995) 15–26.
[14] G. Fuchs, G. Krabbes, P. Schatzle, S. Gruss, P. Stoye, T. Staiger, K.H. Muller, J. Fink, Schultz, Appl. Phys. Lett. 70 (1997) 117–119.
[15] T. Miyamoto, K. Nagashima, N. Sakai, M. Murakami, Supercond. Sci. Technol. 13 (2000) 816–819.
[16] D. Lee, K. Salama, J. J. Appl. Phys. 29 (1990) 2017–2019.
[17] J. Joo, S.B. Jung, W. Nah, J.Y. Kim, T.S. Kim, Cryogenics 39 (1999) 107–113.
[18] W. Lo, N.H. Babu, D.A. Cardwell, Y. Shi, D.M. Astill, J. Mater. Res. 15 (2000) 33–39.
[19] S. Goshima, N. Sakai, M. Takahashi, T. Higuchi, T. Murayama, K. Iida, S.I. Yoo, M. Murakami, Advances in Superconductivity 8 (1996) 739–742.
[20] N. Sakai, A. Mase, H. Ikuta, S.J. Seo, U. Mizutani, M. Murakami, Supercond. Sci. Technol. 13 (2000) 770–773.
[21] P. Diko, S. Takebayashi, M. Murakami, Physica C 297 (1998) 216–222.
[22] M. Kambara, K. Miyake, K. Murata, T. Izumi, Y. Shiohara, T. Umeda, Physica C 330 (2000) 191–202.
[23] A. Endo, H.S. Chauhan, E. Egi, Y. Shiohara, J. Mater. Res. 11 (1996) 795–803.
[24] Japanese Industrial Standards (JIS) R 1625.
[25] H. Fukai, M. Tomita, M. Murakami, T. Nagatomo, Supercond. Sci. Technol. 15 (2002) 1–4.